Simultaneous Detection of Multiple Surface Acoustic Wave Sensor Tags for Water Quality Monitoring Utilizing Cellular Code-Reuse Approach

Kasyap Suresh, Varun Jeoti, *Senior Member, IEEE*, Micheal Drieberg, *Member, IEEE*, Socheatra Soeung, *Member, IEEE*, Asif Iqbal, Goran M. Stojanović, *Member, IEEE*, and Sohail Sarang, *Student Member, IEEE*

***Abstract*—A water quality monitoring application often requires the deployment of Internet-of-Things (IoT) sensors over a wide water body with communication links among them to transmit, receive the data, and then uplink it to the cloud for further analytics. Deployment of this kind requires battery-assisted IoT sensors which require monitoring the battery level and replacement when necessary. It is thus desirable to have battery-free sensor tags and a suitable communication infrastructure to obtain data. In this article, a system that facilitates obtaining sensed data, like pH, through passive sensor tags based on surface acoustic wave (SAW) technology and a cellular code-reuse scheme-based reader infrastructure is proposed. The reader in each cell is able to read multiple sensor tags simultaneously, which itself has been a challenge. The SAW sensor tags are appropriately proposed to be designed to be orthogonal to allow simultaneous detection and the cell range of reader-SAW sensor-tags communication is sought to be further enhanced through a resonant loading of interdigital transducer (IDT)-based reflectors.**

***Index Terms*—Cellular networks, code-reuse, Internet of Things (IoT), SAW pH sensor-tags, scalable networks, sensors, RFID tags, water quality monitoring.**

I. Introduction

THE CONSISTENT surge in human activity over the past century is having a deleterious impact on our environment, at the cost to human health [1]. In many developing countries, the lack of sanitation facilities followed by the activities of mining factories all contribute to negative impacts on the environment. To ensure sustainability, it will be crucial to have efficient monitoring systems for monitoring air quality, water quality, and also for earthquake [2]–[4]. Of particular importance among all is the water quality monitoring (WQM) since every living creature needs water to survive [5]. Although water is abundant on earth, only 2.5% of the available water is fresh water [6] and roughly 20% of the world's population do not have access to safe and clean drinking water [7]. Currently, modernization across urban cities with concentrated human activities are accountable for severe water pollution, which is deemed to be one of the major problems affecting the environment [8]. Hence, detecting and analyzing the pollutants in water is critical. Water quality indicates the generic composition of water in terms of its chemical, physical, as well as biological properties. WQM can be considered as a method for systematically sampling and analyzing the water conditions and its characteristics with time [9]. It typically involves monitoring freshwater sources, such as lakes, ponds, rivers, streams, wells, reservoirs, and wetlands to ensure that the source is providing a safe water for drinking as well as for other human and animal activities [10]. To support the need for why we need to monitor water quality, the spill of a coal processing chemical, 4-Methylcyclohexanemethanol (MCHM) into the Elk river in Virginia, USA is an example that can be used. The river had become contaminated due to this chemical and is located roughly 2.4-km upstream from the public water supply intake for the city in West Virginia. This water contamination was drawn into the city's main water supply stream leaving over 300 000 people and area businesses without water for several weeks. The researchers too had little information on how the spilled chemicals moved in and through the water, and about the toxicity, the measurements, as the relevant published information was either limited or nonexistent [11].

From the 1960s to 2000, WQM mainly relied on a manual approach for water sampling and analysis, where humans would travel to a water source, collect one or more samples, and transport them to a laboratory for further analysis. However, these traditional systems have several limitations, such as high spatiotemporal variability of the physical, chemical and/or microbial parameters of the water, human errors during sample collection, errors introduced by the sample transportation items, and the presence of reagents and other contaminants. Starting from the late 2000s, new technologies were introduced to overcome some of these limitations, such as new sensors that utilized biosensors, optical sensors, and

Manuscript received 28 December 2020; revised 14 April 2021 and 6 May 2021; accepted 14 May 2021. Date of publication 20 May 2021; date of current version 8 August 2022. This work was supported in part by the AQUASENSE Project from the European Union's Horizon 2020 Research and Innovation Program under the Marie Skłodowska-Curie Grant under Agreement 813680, and in part by the Department of Electrical and Electronics Engineering, Universiti Teknologi PETRONAS (UTP). *(Corresponding author: Kasyap Suresh.)*

Kasyap Suresh, Micheal Drieberg, Socheatra Soeung, and Asif Iqbal are with the Department of Electrical and Electronics Engineering, Universiti Teknologi PETRONAS, Seri Iskandar 32610, Malaysia (e-mail: kasyap_16005685@utp.edu.my; mdrieberg@utp.edu.my; socheatra.s@utp.edu.my; asif.iqbal@msn.com).

Varun Jeoti, Goran M. Stojanović, and Sohail Sarang are with the Faculty of Technical Sciences, University of Novi Sad, 21000 Novi Sad, Serbia (e-mail: varunjeoti@uns.ac.rs; sgoran@uns.ac.rs; sohail@uns.ac.rs).

Digital Object Identifier 10.1109/JIOT.2021.3082141

micro electro-mechanical systems (MEMSs) to sense various water quality parameters, such as pH, dissolved oxygen (DO), temperature, and turbidity.

A further improvement took place when wireless sensor networks (WSNs) started gaining increased attention as the communication technologies and techniques improved. WSNs have proven to be very efficient in wirelessly monitoring the environmental data and the ability to acquire and process data from several widely distributed sampling points using low-power communication networks, which assists the decision makers to capture data from multiple remote sensors locations in a timely fashion. In such cases, it is not only the sensed parameter which is needed but also the ID of the sensor since the sensors are widely distributed across different locations. Thus, the sensors can also provide the necessary ID information and hence act as sensor tags where the tag component is used for identifying a particular sensor tag. Several IoT sensors exist among which the silicon-based integrated circuit (IC), a very established technology, is classified into active, passive, and semi-passive. However, these tags suffer from severe multipath reflections in metallic environments [12]. Active silicon tags utilize an internal battery which makes it expensive while passive tags use a rectifier that requires a minimum threshold power from the reader in order to energize them. Furthermore, all silicon-based tags suffer from harsh environmental conditions, such as high temperature, pressure, humidity, and radiation. Compared to them, the chip-less technology, such as surface acoustic wave (SAW) sensor tags are far superior since they can overcome the multipath reflections from metallic environments, can be read under harsh environmental conditions, and can reflect or backscatter at any power level emitted from the reader [13].

SAW tags or sensor tags, unlike silicon-based IC, are one of the kinds of chipless devices and work based on piezoelectricity instead of the semiconductor physics [14], [15]. The SAW tag consists of an input interdigital transducer (IDT), with two interlaced comb-like metal electrodes that is used to transform the incoming electrical signal into 100 000 times slower acoustic waves using any piezoelectric substrates, such as Lithium Niobate ($LiNbO_3$), Quartz, and so on, followed by a series of strategically arranged reflectors that are used to encode ID information in the acoustic waves which is then read by the reader from a distance. Several works have been reported in the area of SAW tags and sensor tags. SAW sensor tags rely on the change in the velocity of SAW wave due to a given sensing variable which, in turn, is measured either as change in resonating frequency of SAW resonator or delay time in SAW delay line. Interestingly, same device can serve both as a SAW sensor as well as a SAW tag [16], [17]. The major difference between SAW sensor tags and SAW tags is that SAW sensor tags include a sensing layer, due to which piezoelectric material parameters, such as velocity, changes when the material properties change due to environmental influences while still providing the tagging information at the same time, unlike SAW tags which provide only the tagging information. Two reflector designs based on orthogonal frequency coding (OFC) and open circuit-short circuit (OC-SC) are available in SAW tags, among which the OC-SC is very popular and commercialized today, mainly due to the provision of large number of codes for a given number of bits and straightforward design [18]. Several work has been carried out in the area of WSNs for WQM among which [19] presents a smart low-cost remote monitoring sensor and utilizes it for performing real-time WQM. Kuang *et al.* [20] described a multiparameter DO prediction model utilizing a collection of water quality sensors and Lambrou *et al.* [21] presented an IoT platform which was applied to conduct water contaminant detection case studies.

With reference to the work in SAW tags, Hartmann *et al.* [22] proposed various anti-collision strategies for SAW tags to improve the detectability. Brandl *et al.* [23], [24] described a reader-based signal processing algorithm based on integer programming and linear block codes using two SAW tags. Zhong *et al.* [25] designed a Barker code-based reflector for SAW tags to mitigate the collision problem. Sorokin and Shepeta [26] proposed a time-frequency strategy for SAW tags with each reflector along a single acoustic path tuned to different frequencies to mitigate intertag interference. In [27], we had discussed an OC/SC IDT-based reflector with a 5-bit binary code design using which a total of 2^5 codes are possible. However, in [22]–[24], the algorithm works well for a very limited number of SAW tags. For cases when more than 1000 SAW tags are to be read, the read time radically increases along with reader complexity and tag-to-tag interference. Barker coded reflectors as in [25] possess good auto-correlation properties but faces severe intertag interference when numerous SAW tags response superpose on each other in the time domain. For the reflector arrangement as proposed in [26] using time-frequency approach, the design works well for a limited number of codes and which are strictly orthogonal. However, for all possible combinations of codes for a given number of bits, there will be an overlap between time and frequency domain which causes several SAW tag responses to superpose on each other resulting in severe intertag interference. In such cases, it is impossible to simultaneously identify numerous tags at the same time. Above all, it is practically impossible to indefinitely increase the number of time or frequency slots in SAW tags as it results in a higher amount of loss and larger delay times. Although OC/SC reflectors can provide us with a larger number of codes in the order of 2^n where n is the number of bits, the number of orthogonal codes that are possible is only n, which is limited, and each reflector located in one of the n possible time slots [27]. Therefore, if all 2^n tags are physically present, all of them cannot be simultaneously detected at a time due to severe intertag interference. Another approach based on frequency-division multiplexing (FDM) for SAW sensors were proposed in [28], but the finite bandwidth limits the number of detectable tags. Time-division multiplexing (TDM) cannot be a solution for SAW devices because the SAW tags or sensor tags, being passive, does not contain sophisticated functionalities to pseudorandomly delay the responses so as to avoid interference due to multiple tags. Hence, a fast and error-free detection approach is needed to detect numerous ($>10^4$ or 10^5) orthogonal SAW sensor tags so that a practical number of items can be simultaneously read over a wide area.

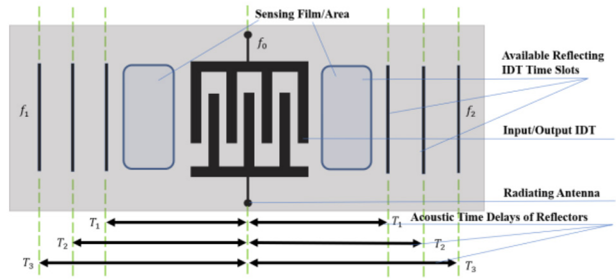

Fig. 1. Typical SAW sensor-tag design.

A typical SAW sensor-tag design is shown in Fig. 1 where a sensing layer is deliberately added followed by a series of coding reflectors. Thus, a SAW sensor tag is a single device that performs both sensing as well as tagging (or identification) at the same time. The tag detection is carried out by detecting the peaks obtained after receiving the reader signal back at the reader and correlation. The error probability versus SNR plots are obtained, and the error probability is used to estimate the cellular radius of the reader system.

In this article, we make use of a SAW sensor tag that performs both sensing of pH value as well as tagging utilizing a time-frequency lattice ID as in Fig. 1. ZnO-based pH sensing principle is sought to be utilized as in [29]. A similar design is presented in Section IV and is used to explain the WQM scenario. The study is focused on simulation-based feasibility study of a cellular-based reader system design that can simultaneously read multiple SAW sensor tags at a time. Accordingly, the sensor tags were not needed to be bought and physically tested.

In the light of the above, the scope and contributions of our article are as follows. Comparing with [19]–[27], we present a novel and efficient approach to WQM using cellular code reuse and to simultaneously identify, and, implicitly, sense multiple orthogonal SAW sensor tags. The so-developed approach is intended to monitor the water quality over a wide-area pond, lakes, rivers, and coastal sea where many water-based assets and other resources may lie. In this method, multiple SAW sensor tags and readers are strategically divided into several hexagonal cells that form a cellular infrastructure and by appropriately maintaining the distance between the same group of SAW sensor tags across different cellular hexagonal regions, the intertag interference between the same group of codes can be easily avoided. Using the cellular code-reuse approach in conjunction with our SAW sensor tag, the number of orthogonal SAW sensor tags can be significantly scaled-up, thereby allowing a greater number of them to be deployed on water bodies over a very wide area. Our article is further organized as follows. Section II explains the code-reuse technique for reader-SAW sensor tags/tags. Section III explains the SAW tag and sensor-tag model based on time-frequency lattice approach. Section IV describes a WQM scenario in a large pond which utilizes the cellular code reuse with orthogonal SAW sensor tags. Sections V explains the various reflector load conditions. Section VI presents the simulation results for the time-frequency lattice, S_{11} in time and frequency domain followed by the peak detection and read range analysis. Finally, we conclude and provide future directions in Sections VII and VIII.

II. Cellular Code-Reuse System

Inspired by the frequency reuse concept of cellular networks [30] currently applied to the present mobile devices which relies on an intelligent allocation and reuse of frequency channels throughout a cell coverage region, the code reuse approach follows a similar approach on an intelligent allocation and reuse of ID codes of tags throughout the coverage region and is a relatively new realization for tag-reader systems. Although a similar but different concept is explained earlier [30], we attempt to explain it with a code-reuse-based perspective such that the explanation fits the context. This approach is equally applicable for SAW sensor tags too. However, the concept was explained using tags to explain the intelligent reuse of tag IDs across various hexagonal cells over a wide area. Unlike the frequency reuse concept where there are cellular base stations present in every hexagonal cells covering a finite number of selective subscribers, code reuse approach follows similar standards except that the base station is replaced by a reader. In this approach, each cellular reader is allocated a group of SAW tag codes to be used within a small geographical area called a cell. Readers in adjacent cells are assigned ID codes which contain completely different codes than the neighboring cells. The reader antennas are designed to achieve the desired coverage within the cell. By limiting the coverage area to within a cell, the same group of tag ID codes can be used to cover cells that are separated from one another by distances that are large enough to avoid the collision of tags. The design process of selecting and intelligently allocating the code groups for all readers within a cellular system is called code reuse or code planning. Fig. 2 illustrates the concept of code reuse where the readers labeled with the same letter use the same set of codes.

The hexagonal cell shape as shown in Fig. 2 is a conceptual and simplistic model of the radio coverage for each RFID reader, but it has been universally adopted since the hexagon permits a larger radio coverage area in conjunction with no overlapping regions relative to a circle [30]. Other shapes, such as squares and rectangles provide a lesser area for a given side length relative to a hexagon, which makes hexagon an appropriate choice. When using hexagons to model coverage areas, RFID readers are depicted as either being in the center of the cell or on any three of the six vertices. Usually, isotropic antennas are used in center while sectored-directional antennas are used as corner-excited cells.

To understand the code-reuse approach, consider a cellular system which has a total of C codes available for use. If each cell is allocated a group of n codes ($n < C$), and if the C codes are divided among M cells into strictly unique and disjoint code groups and each having the same number of codes, then the total number of available ID codes can be expressed as in the following equation:

$$C = nM. \tag{1}$$

The M cells which collectively use the complete set of available codes is termed as a cluster. If a cluster is replicated or reused K times within the system, the total number of codes, N, can be used to measure the entire capacity of the cellular

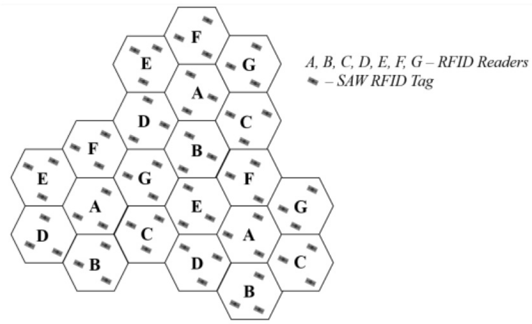

Fig. 2. Typical cellular code reuse framework with $M = 7$ cells per cluster.

RFID system and is given by the following equation:

$$N = KnM. \tag{2}$$

By substituting (1) in (2), we obtain the result as in the following equation:

$$N = KC. \tag{3}$$

From (2), the code capacity of a cellular RFID system is directly proportional to the number of times (K) a cluster is reused within the fixed interrogation area. The factor M is called the cluster size and is typically an integer number. If the cluster size M is reduced while keeping the cell size constant, more clusters are required to cover the given area and hence more code capacity can be achieved. Generally, a larger cluster size implies that the ratio of cell radius to the distance between co-channel cells is high. Conversely, a smaller cluster size explains that the ratio is small and that the two co-channel cells are located closer together. The code reuse factor of a cellular RFID system is given by $1/M$, since each cellular reader within the cluster is allocated only $1/M$ of the total number of available ID codes in the system. Fig. 1 shows an illustration of a total of 63 SAW tags deployed over a given wide area although the entire $M = 7$ cell cluster contains only 21 orthogonal SAW tags.

A. To Find the Appropriate Hexagonal Cell to Reuse the Same Group of SAW RFID Sensor-Tag Codes

Since the geometry contains six equidistant neighbors per cluster and that the lines joining the centers of any cell and every other neighbor are separated by 60° and multiples of it, not all cluster sizes and cell layouts can fulfil this criterion. The appropriate hexagonal cell to be chosen for reusing the same group of codes is satisfied by the following equation in [30]:

$$M = i^2 + ij + j^2 \tag{4}$$

where i and j are nonnegative integers. The above equation provides the number of hexagonal cells to be used within a cellular system while maintaining the code-reuse distance necessary to keep the same group of codes at a sufficiently large distance to avoid tag-to-tag interference. To find the nearest cell where the same group of codes are used, a set of procedures has to be followed: 1) move i cells along any chain of hexagons such that the centers are joined along the line passing through it and 2) turn 60° counter clockwise from the earlier direction of movement and move j cells. For instance, in Fig. 2, the group of codes used by reader A can be reused by two cells along the chain of hexagons ($i = 2$) and moving one cell ($j = 1$) upon turning 60° counter clockwise from the earlier direction. This will provide us the cell at which the same group of codes can further reused, which maximizes the capacity of the cellular RFID system. The minimum distance required to reuse the same group of ID codes is called the code-reuse distance and is given by the following equation [30]:

$$D_{\text{reuse}} = \sqrt{i^2 + ij + j^2}.R\sqrt{3} \tag{5}$$

where the factor $R\sqrt{3}$ is the distance between the centers of any two adjacent cells. Upon substituting (4) in (5) we obtain the result

$$D_{\text{reuse}} = \sqrt{M}.R\sqrt{3} = \sqrt{3M}.R \tag{6}$$

where R is the radius of a cell. Although the time slots of SAW RFID tags or sensor tags cannot be indefinitely increased, the code-reuse approach allows us to intelligently allocate the same group of codes according to a predetermined set of rules as explained previously. In the subsequent sections, we present a SAW sensor-tag layout which will be utilized for the WQM system framework. In Fig. 2, since there are also multiple readers co-located within and throughout cells, the reader-to-reader interference will be inevitably present and can be resolved by utilizing an appropriate protocol [31]. With the combination of the above techniques, it is feasible to orthogonally scale-up the number of orthogonal SAW sensor tags by reusing the same group of codes in another cell which can significantly maximize the number of orthogonal codes.

III. Time-Frequency Lattice Design of SAW Sensor Tags

Fig. 3 illustrates the proposed time-frequency lattice design for a SAW tag. In this design, the acoustic paths are present on either side of the input/output IDT unlike other SAW tag designs where the input/output IDT typically radiates along a single acoustic path which is present in the right side of the input/output IDT.

The input IDT is connected to the antenna which receives the electromagnetic (EM) waves sent from the RFID reader. The antenna sends this signal to the input IDT which converts the electrical energy into acoustic energy. This acoustic energy E with bandwidth B, before propagating, is split bidirectionally into energies of energy ($E/2$) and bandwidth ($B/2$) and propagates on either side of the IDT. Various choices for the piezoelectric substrates exist, e.g., $LiNbO_3$, Quartz, multilayer substrates, and so on. In the proposed design, the input IDT transmits a wideband signal centered around a frequency f_0, while the reflecting IDTs present on either side resonate at two different frequencies $f_1 = f_{0-B/2}$ and $f_2 = f_{0+B/2}$ with bandwidths equal to ($B/2$). These energies get reflected from n_t equispaced reflectors on either side. The delay values from reflectors on either side are the same. The output IDT (the input IDT also acts as output IDT) receives these successive reflections from both the paths and upon converting them into

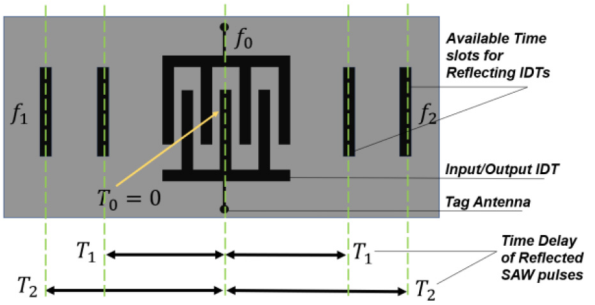

Fig. 3. 2-bit time-frequency lattice design for SAW RFID tags.

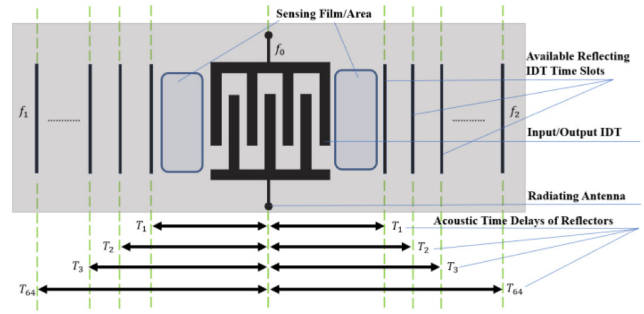

Fig. 4. 64-bit time-frequency lattice design for SAW sensor tags.

electrical signals, is backscattered at the antenna to the RFID reader. The RFID reader antenna receives the EM signal and is analyzed in the time-frequency lattice. As shown in Fig. 3, it is possible to analyze the signal in two different dimensions (or domains) because the reflectors which are spaced at equal time slots in both the acoustic paths can also have either of the frequencies at any given time instant. Hence, there is a unique combination for a given SAW tag design. The proposed design exploits a single reflector IDT per SAW tag which gives rise to only one reflection at any given time instant T_1 or T_2 with frequency f_1 or f_2. This gives rise to a single unique signature for one SAW tag which will be strictly orthogonal to other SAW tags in the time-frequency lattice as in Fig. 3. Here, the word orthogonal indicates there is no relationship of the IDs of any two SAW tags and are unique to each other.

The use of time slots and two frequency bands thus creates a time-frequency lattice. Each point in the lattice is reflective of reflection from some reflector in either frequency band. Associated with one object, it gives the object a unique time-frequency slot that cannot be mixed with any other slot and, hence, stays orthogonal to other time-frequency slots. In other words, the time frequency index can act as unique ID identifier orthogonal to other indices. The generatable number of SAW tags for a given number of time slots is straight forward to obtain. For instance, a 2-time slot and two frequencies, would contain $2 \times 2 = 4$ possible number of SAW tags. Similarly, 3, 4, and 5-bit time slot designs can generate a total number of 6, 8, and 10 orthogonal SAW tags. Thus, for any given n_t time slots and n_f frequencies, the total number of perfectly orthogonal SAW tags that can be generated is given by

$$N_{\text{orthogonal}} = n_t \times n_f \tag{7}$$

where $N_{\text{orthogonal}}$ is the total number of perfectly orthogonal SAW tags that can be simultaneously detected at one time. Our proposed tag design is such that there exists only a single reflector for the designed time-frequency lattice for a single tag. This reflecting IDT contains a unique time-frequency index that is strictly orthogonal to other indices attached to other SAW-ID tags. As a result, when several of them reflect their ID codes, the time-frequency lattice response can efficiently distinguish a single SAW tag in the midst of several tags. With this design, any number of SAW tags or all of them can be simultaneously detected at the same time over a wide area with just a simple reader design and a single antenna. Furthermore, the intertag delay which results when the tags are present at different locations does not play any significant role because the intertag time delay is due to EM RF waves which is relatively smaller than the delay of acoustic waves and appear to arrive together.

Fig. 4 shows an extended illustration of a time-frequency lattice design for a 64 bit. Unlike Fig. 3, the design proposed in Fig. 4 contains a sensing film/layer too. This sensing film can be used to sense and measure physical and chemical parameters of external environments, such as temperature, pressure, humidity etc. The design also contains a unique ID such that every SAW sensor tag backscatters a sensed value along with its ID which is used to confirm its presence to the reader. By utilizing this design, a total of 128 orthogonal SAW sensor tags will be possible. The following section presents a real-time application scenario for the purpose of WQM where the proposed SAW sensor-tag design in Fig. 4 will be adopted. The application of proposed cellular code reuse with orthogonal SAW sensor tags for WQM will be detailed.

IV. Proposed Novel Water Quality Monitoring System Framework Utilizing Cellular Code-Reuse Approach and Orthogonal SAW Sensor Tags

This section demonstrates the way in which WQM in areas, such as a large pond can be performed using wireless network of passive SAW sensor tags which measure the pH value instantaneously. A typical scenario of a large pond where several SAW sensor tags are strategically arranged in a cellular fashion is shown in Fig. 5. This section aims to show that by utilizing the time-frequency lattice-based design of SAW sensor tags in conjunction with cellular code-reuse approach, numerous sensor tags can be simultaneously deployed and detected at the same time with multiple readers which provide both the sensed pH of the water quality and the identification signature of the SAW sensor tags. Furthermore, the data can be uploaded by the readers to the cloud using suitable wireless technologies.

SAW sensors consists of waves traveling along the surface of a material exhibiting elasticity and since the acoustic energy is confined in the near-surface region of the solid, the sensitivity is higher due to various surface perturbations on the acoustic wave [32]. Tang *et al.* [29] physically designed a ZnO-based SAW pH sensor where no reference electrodes are required for sensing [29]. The pH value is sensed based on the interaction between hydronium (H_3O^+)

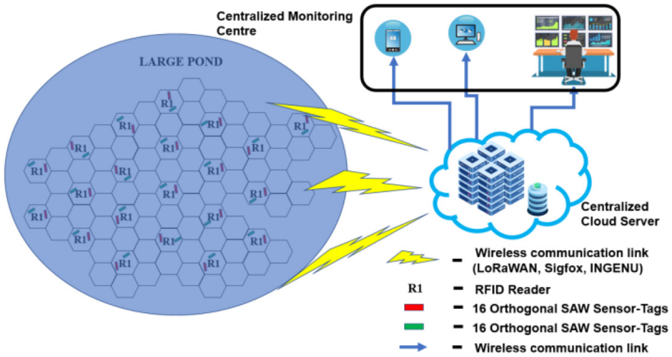

Fig. 5. Framework of WQM system utilizing cellular code reuse with several orthogonal SAW sensor tags deployed over a large pond.

or hydroxide (OH^-) and ZnO. We assume, the same design sensing principle can be used for pH measurement in the proposed SAW sensor tag for WQM. As for the tag design, the time-frequency-based lattice design approach is as explained in section *B* later. By utilizing the technique of cellular code reuse in conjunction with time-frequency lattice design, a wide-area pond or a lake can be wirelessly monitored and several SAW sensor tags can be simultaneously detected and sensed using multiple readers in real-time, allowing to measure the quality of water based on pH measurements [29]. Therefore, the presented WQM system is also practically realizable.

A. Sensing Principle and Fabrication Steps of a ZnO-Based SAW pH Sensor Tag

The pH value of water can be determined from the SAW sensor-tag sensing operation as follows. SAW waves are accompanied by an electric potential wave which results in the electric polarization of dipoles due to the mechanical deformations of the piezoelectric material through electroacoustic effect. These electric fields interact with different carriers close to the material surface. This, in turn, influences the propagation characteristics of the acoustic wave which alters the wave velocity. The pH-based behavior of the ZnO layer can be explained in terms of electrochemical potential at the ZnO and water interface. The ZnO surface becomes polar by the adsorption of pH dependent hydroxyl or hydronium ions which, in turn, causes a resulting change in voltage at the electrode/water interface. The interaction of this pH dependent so-developed electrochemical potential with the electric potential wave that is associated with the acoustic wave in piezoelectric substrate causes a proportional change in the phase velocity of the acoustic wave [29], [33]. This change in phase velocity is, in turn, reflected in terms of change in resonance frequency or excess delay time which is easy to measure. The excess delay times can be measured by utilizing a reference sensor in the design of the sensor tag using which any difference in this parameter can be estimated. This difference directly affects the pH value which can be easily measured. In the proposed ZnO-based SAW pH sensors, these excess delay times are measured by the reader, and this information is sent to a cloud server for constructing the map of pH values of the water over the intended waterbody.

Since each hexagonal cell contains a reader and there are other readers nearby, and if a backhaul is used to carry the data to ground before uplinking to a centralized cloud server, the issue of reader-to-reader interference or cross-talk between readers can also be addressed by choosing an appropriate protocol [31]. This article proposes to utilize pH as the sensing parameter by analyzing the relationship between the delay time and the change in pH. However, other sensing parameters do exist and can also be used to quantitatively measure the water quality namely the turbidity, oxidation reduction potential (ORP), electrical conductivity, temperature, salinity, and chlorophyll-a concentration [34], [35]. For the case when multiple parameters are to be targeted, one sensor tag for one parameter approach has to be used. Accordingly, the design of SAW sensor tag has to be modified to suit the appropriate parameter measurement individually. A single SAW sensor tag is not expected to measure multiple parameters at the same time. As per the design Fig. 4, the design is for a single variable sensing device which acts as a sensor tag and hence the reader will read both the sensed variable as well as the ID information because the SAW wave contains both information (sensing and tag ID).

The fabrication steps of the proposed SAW sensor tag can be carried out as follows. The electrodes in the IDTs can be made of Au (Gold). The fabrication process starts with radio frequency (RF) sputter-deposition of ZnO thin film atop the silicon base substrate [29]. Second, the Au electrodes can be deposited using electron-beam evaporation and using photolithography and lift-off technique patterned atop the ZnO thin film. This method is applicable for both sides of the input/output IDT [29].

B. Applying Cellular Code-Reuse Approach With Time-Frequency Lattice Detection

For demonstrating this application scenario, we utilize the SAW sensor-tag design as shown in Fig. 4. The piezoelectric material is chosen as ZnO [29] for illustrating the application feasibility. Therefore, it is justifiable to utilize a SAW sensor for the purpose measuring the pH value of water for the above mentioned scenario. From the design shown in Fig. 4, a total of 128 orthogonal SAW sensor tags are possible to generate according to (7).

The SAW sensors-tags are not submerged under the water for sensing. However, a mechanical pipette or tube is connected to the SAW sensor-tag [29]. The two ends of the pipette or tube are underwater which is used to collect the water samples above water body. These samples are then allowed to interact with the SAW sensor tag and to the sensing film. The SAW sensor tags are actually placed on top of the water surface and can be so designed that the antenna points toward the air or the sky which does not allow the antenna to come in touch with the water. Therefore, the SAW sensor tags do not radiate any RF waves inside the water and hence no radio communication takes place under the water. Hence, the tuning of the SAW sensor-tag antenna is not required for this system. Multiple RFID readers will also be deployed on top of the water surface. Since the SAW sensor tags are

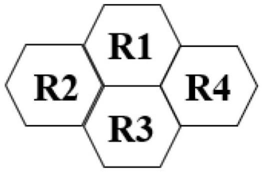

Fig. 6. Cell cluster $M = 4$ consisting of a single reader and 32 orthogonal SAW sensor tags per hexagonal cell. Total number of orthogonal codes for entire cluster = 32 (n) × 4 (M) = 128 (C).

passive/battery-free by design, power is generated using the backscatter principle where the RFID reader probes them with a chirped signal. The SAW sensor tag, unlike its silicon-based counterpart, does not require a rectifier circuit to extract energy from the signal and can directly receive the signal transmitted by the reader and convert it into slower acoustic waves on the piezoelectric substrate. Thus, the RFID readers generate the power and energy which is then used to activate and energize the SAW sensor tags. The SAW sensor tags in turn utilize this energy to encode the necessary sensed information and the ID code which is then "backscattered" back to the RFID reader.

Fig. 6 shows a cell cluster consisting of four hexagonal cells where each reader occupies a cell. Each cell consists of 32 orthogonal SAW sensor tags which will be simultaneously read by a reader in that cell. Therefore, the cellular cluster consists of four readers and since $M = 4$, the total number of orthogonal SAW sensor-tags per cell cluster is 128. Consider that these 128 SAW sensor tags are floating above the water surface while connected to the pipette. The reader consists of two components which are namely 1) for reading SAW sensor tags and 2) for sending the information to an external centralized cloud server.

The reader can afford to use any existing wireless technology, such as low-power wide area network (LoRaWAN) or other WiFi/4G/5G Internet-of-Things (IoT) backbone technologies [36] when considering applications, such as on sea-like waterbodies where a base station might be required as a gateway to communicate with a cloud server since the signal has to propagate off-shore and over long distances (in the order of km) from the readers. However, for this application scenario where a large pond is considered, the readers can transmit the sensed and ID information of all SAW sensor tags to the cloud server directly via LoRaWAN and/or WiFi-like technologies. A survey and review on utilizing WSNs for WQM is provided [36], [37].

Let us assume that an RFID reader is placed in the middle of a hexagonal cell with its fixed number of stationary sensor tags in its range. The reader emits a linear frequency modulated (LFM) up-chirp (frequency increases linearly with time) signal of constant magnitude throughout the time duration. We also consider that the reader emits this up-chirp signal at a center frequency of 2.25 GHz with a transmit power of 10 mW, an antenna gain of 10 dBi, and that all the SAW sensor tags possess an antenna gain of 7 dBi. The power requirement as per the federal communications commission (FCC) rules for ultrawideband (UWB) is strictly within the power limits since the maximum transmit power does not exceed 100 mW [38]. The read range results presented in section VI also utilize the parameter values as mentioned above. Also,

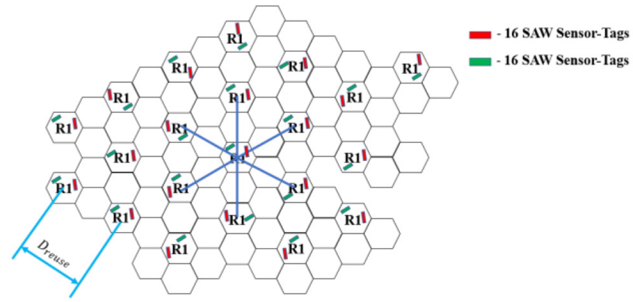

Fig. 7. Cellular code-reuse framework with $M = 4$ cells per cluster where same group of codes are reused 21 times ($K = 21$) giving rise to 128 (C) × 21 (K) = 2688 (N) orthogonal SAW sensor tags.

assume that each reflector is spaced 50 ns apart from each other followed by a 50 ns delay between the first reflector time slot and the input IDT. From those assumptions, it is clear that the acoustic time delay between the first SAW sensor tag and the input IDT is 200 ns. Similarly, other SAW sensor tags are present in the remaining 63 reflector time slots in either of the frequencies f_1 or f_2. When the reader emits an interrogation pulse, the signal is received by all the SAW tag antennas.

The input/output IDT is directly coupled to the antenna which receives this EM wave and converts it into a 100 000 slower SAWs that propagates along the piezoelectric material. The acoustic waves then reflect off from those shelf ID as well as the tag ID reflectors and are then received by the output IDT which reconverts the acoustic waves into an electrical signal. The 128 SAW tag-IDs are received by the output IDT after a delay time of T_1 for tag-1, T_2 for tag-2, and up to tag-128 at T_{64} as shown in Fig. 4. These IDs are backscattered to the RFID reader which receives these ID codes at different times because each tag is located at a distance different from others. Thus, the total propagation time is the sum of the time taken to travel from the tag-to-reader antenna and the delay time of SAW tags.

Assume that the SAW sensor tags are located at different distances with tag-1 at 1 m, tag-2 at 2 m, tag-3 at 5 m, tag-4 at 6 m, and up to tag-128 which is at 10 m. This corresponds to a EM delay time of 3 ns, 6 ns, 16 ns, 20 ns, and 30 ns. But the SAW waves arrive at the reader only after a delay sufficient enough before all the environmental echoes die away. If T is the SAW delay time defined by $T \in \{T_1, T_2 \ldots \ldots, T_{64}\}$ where each element in the array represents the corresponding time delay for every SAW tag, then the total propagation time T_{total} is $\{3\text{ ns}, 6\text{ ns}, 16\text{ ns}, 20\text{ ns}, 30\text{ ns}\} + T$. This total time is sufficient enough for all the environmental multipath echoes to die out before the SAW waves arrive at the reader. When reader receives the SAW tag responses and analyzes it in the time-frequency lattice, the lattice response will appear as shown in Fig. 8.

From Fig. 8, tag-1 can be easily differentiated from the other SAW tags that are also simultaneously present in the response. Here, each SAW tag contains its own time-frequency lattice signature which is unique to other SAW tag IDs. Since the SAW tags are located at different distances, they all arrive at different times and with different signal-to-noise ratio (SNR)

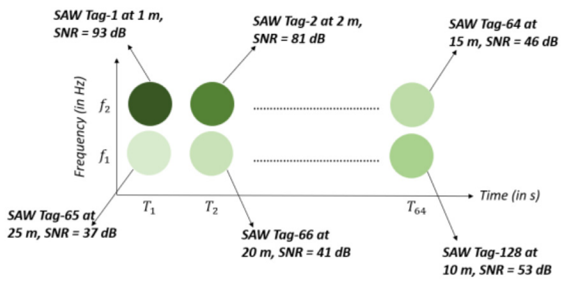

Fig. 8. Typical 64 × 2 time-frequency lattice detection response for one cell cluster consisting of four readers and 128 orthogonal SAW sensor tags.

values. Hence, the fade of the green dot is different for different SAW tags due to varying SNR where the tag with a higher SNR is darker than the tag with a lower SNR (a lighter dot). The parameter values in Fig. 3 are estimated using (15) in the light of the parameters in the results and discussion section.

Now that the strategy for deploying 128 orthogonal SAW sensor tags is performed, the advantage of cellular code-reuse approach has to be realized in order to derive maximum benefit in terms of the wide area tag deployment. Since the number of cells per cluster is $M = 4$, only $i = 2$ and $j = 0$ (or *vice versa*) are the possible solutions that fit the equation expressed in (4). This means that from any reader R1 in a cell, we have to move two cells across in any direction which results in a cell where the same group of codes can be reused. Similar procedure can be adopted for the remaining three readers R2, R3, and R4. Hence, in this manner, the entire cluster is now reused two times which results in $128(C) \times 2\ (K) = 256(N)$. The distance D_{reuse} is the distance at which the same group of codes can be reused. This ensures that the tag-to-tag interference is avoided because they are spatially separated such that the given tag of one cell will not interfere with the tags of same code from adjacent cells and vice-versa. If the cluster is reused again, following above reuse procedure yields us a total of 384 orthogonal SAW sensor tags.

C. Scalability of Cellular Code-Reuse Approach

Thus, by following the same procedure, if the same group of codes in the cluster are reused 10 times ($K = 10$), then we obtain a total of 1280 orthogonal SAW sensor tags. Reusing them with $K = 1000$ yields 128 000 orthogonal codes. To cover an even wider area of the pond, by substituting $K = 10\,000$ in (3), we obtain a total of 1 280 000 orthogonal SAW sensor tags which is roughly 1.3 million orthogonal sensor tags that are deployed over a wide area in the pond. It is implied that with the growing number of SAW sensor tags, the number of readers is also increased every time a new cell cluster is added in the scenario. These sensor tags can be simultaneously read at a time by multiple readers over a wide area by using the time-frequency lattice detection approach. The cellular code-reuse approach can be applied to any number of bits in the SAW tag and can also be scaled-up to millions of orthogonal codes even with a 2-bit design as in Fig. 3.

Thus, from the analysis carried out in Sections IV-A–IV-C, it is evident that the proposed approach allows us to scale-up the number of orthogonal SAW sensor tags to any figure of interest, without causing any tag-to-tag interference. The readers can upload the sensed data to control center using a time-division multiple access approach to avoid cross talk among them. This means that every reader simultaneously reads the assigned group of SAW sensor tags and uploads the same in a time-division multiplexed fashion such that no reader-to-reader collision takes place. Since, the SAW sensor tags are passive in nature, they cannot pseudorandomly delay their responses in a TDM fashion. Hence, no special paging signal for the sensor tag is required. Also, there is no frequency shifting across cell boundaries as every cell uses the same frequency band and no sensor tags are moving. The system, as a whole, leads to a wide-area density of SAW sensor-tag deployment where multiple readers and SAW sensor tags are present and the cross-talk between readers is addressed via an appropriate TDM-based protocol [31]. The tag code collision between different SAW sensor tags is also addressed by utilizing our proposed cellular code-reuse approach while the interference from other codes in the same cell is minimized by an orthogonal design of the codes. As a result, a simultaneous detection of multiple SAW sensor tags is feasible via multiple readers and over a wide area.

V. Read Range Improvement Using Resonant Loading of IDT-Based Reflectors

It can be shown that a resonantly loaded IDT using an inductor acts as a better reflector for SAW tags compared to open circuit (OC) reflector design due to their relatively higher magnitude of reflection. But it is necessary to analyze the load conditions mathematically as a theoretical validation before observing the simulations of the loading conditions.

A. Reflected Power Analysis for Different Load Conditions When Using IDT as a Reflector (or Reflecting IDT)

The reflected power of a SAW tag design is important because it provides a meaningful estimate of the reflection that can be expected from the reflector IDT. The reflection magnitude for both OC, SC and inductive loading condition is provided in the following paragraphs as a method to mathematically validate that a resonantly loaded reflecting IDT reflects off a higher energy relative to an OC reflector and hence proves to be a relatively better reflector compared to existing reflector designs in SAW tags.

1) Open Circuit Load, $Y_L = 0$: The general equation for the reflected power in terms of the P-matrix P_{11} [26] is given in the following equation as:

$$P_{11}(Y_{\text{L}}) = P_{11,sc} + \frac{2P_{13}^2}{P_{33} + Y_{\text{L}}} \tag{8}$$

where the term Y_L is the load admittance or simply the load connected across the reflecting IDT as in Fig. 9, P_{13} is an electrical parameter, P_{33} refers to the admittance which is given by $j\omega C_t + G_a + jB_a$, where C_t refers to the total static capacitance, G_a is the radiation conductance, B_a is the acoustic susceptance, and $P_{11,sc}$ is the short-circuit reflection power. Hence, for $Y_L = 0$, (10) becomes

$$P_{11}(Y_{\text{L}}) = P_{11,sc} + \frac{2P_{13}^2}{(j\omega C_T + G_a)} \tag{9}$$

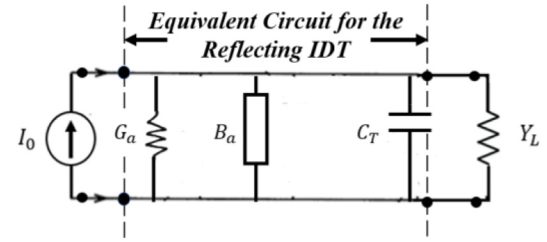

Fig. 9. Load Y_L connected across the reflector to control the reflection [39].

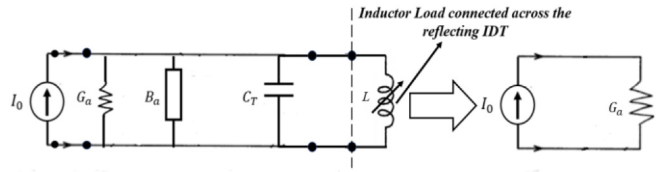

Fig. 10. Inductor load connected across the reflecting IDT.

where B_a is always 0 at frequency f_0. This indicates that the reflecting IDT when open-circuited, will reflect-off a finite amount of power after being received and absorbed.

2) Short Circuit Load, $Y_L = \infty$: We now consider the situation when the IDT reflector circuit is closed, i.e., short circuit (SC) condition. When there is a short-circuit, a small or an infinitesimally small amount of reflection propagates from the IDT reflector. At $Y_L = \infty$, (10) becomes

$$P_{11}(Y_\mathrm{L}) = P_{11,sc}. \tag{10}$$

This indicates that the reflection is very small from the reflecting IDT relative to the OC condition with a reduction in the reflection by a factor of $2P_{13}^2/P_{33}$. Another terminology for OC/SC-based reflector design is pulse position modulation (PPM) or simply on-off keying (OOK), though in this case, an "off" condition does not necessarily mean a zero magnitude reflection but is used as a means to describe the general principle behind the design.

3) Inductive Resonant Loading Load, $Y_L = (j.\omega_o L)^{-1}$: Finally, we consider a special case when the reflecting IDT is resonantly loaded with an inductor. Note that the inductor is connected externally across the reflecting IDT as in Fig. 10. This cancels out the capacitive effect that usually causes a loss in the reflection. Thus, (10) becomes

$$P_{11}(Y_\mathrm{L}) = P_{11,sc} + \frac{2P_{13}^2}{\mathrm{G}_a}. \tag{11}$$

The above equation shows that the term $j\omega C_t$ has been cancelled out from (11) due to the elimination of capacitive effect at the resonant frequency f_0. The explanation for capacitive effect is as follows. As seen from the input source (voltage or current), there is a frequency dependent mismatch of impedance. This means that the source and load impedances are not matched properly because one of them contains a reactive component while the other acts as a purely resistive element. Therefore, in order match the impedances of both source and load, an equal but opposite reactance has to connected across so that the reactance components cancel out each other. Since, both of them are frequency dependent, they cancel out only at a particular frequency called resonant frequency denoted by f_0. Once the circuit is matched, maximum power/energy is delivered from source to the load.

Hence, upon resonantly loading the reflector with an inductor, only the term G_a is present in the admittance which provides a maximized power relative to the OC design. This also indicates that there is an additional power that reflects back once the IDT receives and absorbs the energy. Assuming dynamic switching of SAW RFID tags, the open and SC conditions do not differ a lot in geometry except that the switch is open which releases the incident SAW waves, absorbs, and reflects back. Hence, a finite reflection occurs for this type of reflector. For SC, a bonding wire or a bus bar is connected which run in parallel and the switch is closed, thus creating a very little or no reflection from the IDT reflector relative to OC reflector. For the case of inductive resonant loading (IRL), more power is being reflected off from the reflector. The amount of power reflected from it provides a numerical way to analyze and evaluate the performance of such designs. This in turn proves to be useful in further improving the design and performance of SAW-ID tags. The value of inductance L from the inductor must be chosen such that it eliminates the capacitive effect at the resonant frequency and is given by

$$L = \frac{1}{(\omega_o)^2.C_t} \tag{12}$$

where ω_o is the angular frequency and is given by $2\pi f_o$. L is the inductance (in H), and C_t is the total static capacitance of the IDT reflector and is equal to $C_S.H_a.N_p$, where C_S is the static capacitance per finger pair per cm, H_a is the acoustic aperture of the IDT reflector, and N_p is the number of finger pairs of the IDT reflector. This design has been proved to be very useful in terms of obtaining a higher magnitude of reflection relative to the OC/SC-based reflector design where a resistive loading is employed to control the reflection magnitude. With this theoretical framework, the following section will present the simulations based on the loading conditions.

VI. Design Validation, Results, and Discussion

A. Design Validation Based on the Existing Work

Prior to modeling our SAW tag using time-frequency approach, we have designed and validated our model in [27] on range maximization based on the published work [40]. The operating frequency and bandwidth were borrowed from [40] to validate and show the superiority of our design. An OC design for SAW tag was carried out. A reproduction of S_{11} reflection loss for an OC-based single reflector was performed and shown in [27] for the same design and parameters as in [40]. We had estimated a reflection loss of exactly −30 dB using coupling-of-modes (COMs) modeling which agrees with the result presented in Fig. 7 in [40] which shows that our design methodology is accurate.

B. RFID Reader and SAW Tag Design Parameters

Various design configurations were developed for SAW RFID tags for the UWB technology using the COM theory and relevant simulations were undertaken by developing the Transmission matrix equations for the input/output IDT, delay line, and for reflecting IDTs [39], [40]. The COM modeling is a universal model for simulating SAW devices and is so mathematically designed that it presents a very valid and accurate representation of the design performance of any SAW device. Hence, the validation of the results was carried out using the COM theory itself. Additionally, probability of error versus SNR analysis based on peak detection for the single reflector was also performed for feasibility of detection. The simulations are analyzed using the reflection loss S_{11} in time and frequency domain and a separate time-frequency analysis. Upon computing the S_{11}, a bandpass filter is applied to the incoming signal from the SAW tags such that the two frequencies f_1 and f_2 are separated and plotted as time-frequency plots. An up-chirp LFM signal was transmitted from a single antenna RFID reader at $f_0 = 2.25$ GHz and Bandwidth $(B) = 500$ MHz [40]. Upon reaching the tag, the energy is split into two equal energies at the input IDT with equal bandwidths $(B/2) = 250$ MHz and frequencies f_1 and f_2 centered at 2.125 GHz and 2.375 GHz.

The design parameters for input/output IDT are as follows: $f_0 = 2.25$ GHz, 128° Y-X cut $LiNbO_3$ as the piezoelectric substrate with substrate velocity $(V_0) = 3997$ m/s, capacitance per finger pair per cm $(C_s) = 0.5$ nF, Bandwidth, $B = 500$ MHz and chosen according to the FCC standards of UWB technology requirements [38], acoustic aperture $(H_a) = 100\lambda_0$, number of finger pairs $(N_p) = 4$, width $(w) = 6.46$ μm and electrode thickness $(h) = 150$ nm. The design parameters for the reflectors in the left side of the input IDT are as follows: $f_1 = 2.125$ GHz, $(B/2) = 250$ MHz, $H_{a1} = 83\lambda_0$, $w_1 = 14$ μm, $N_{p1} = 8$, and electrode thickness $(h_1) = 150$ nm $= h$ and similarly the design parameters for right sided reflectors include, $f_2 = 2.375$ GHz, $(B/2) = 250$ MHz, $H_{a2} = 79\lambda_0$, $w_2 = 14$ μm, $N_{p2} = 9$, and $h_2 = 150$ nm $= h_1 = h$. The inductance L used for resonant loading for the frequencies f_1 and f_2 is given by 8.96 and 7.55 nH. The corresponding total static capacitance values are given by 0.63 and 0.59 pF, respectively. The round trip time for the first and second location reflectors are 100 and 200 ns, respectively. This corresponds to the first reflecting IDT located roughly 400 μm and the second reflecting IDT located roughly 800 μm from the input IDT.

As far as the reader-tag communication is concerned the relevant parameters are as follows: reader transmit power $(P_t) = 10$ mW (within FCC limits), reader antenna gain $(G_{\text{reader}}) = 10$ dBi, tag antenna gain $(G_{\text{tag}}) = 7$ dBi, signal integration time $(T_i) = 1$ ms, noise figure (NF) $= 5$ dB, SNR $= 12$ dB and 17 dB, Boltzmann's constant $(k) = 1.38 \times 10^{-23}$, absolute temperature $(T_0) = 300$ K, and losses due to SAW tag $(L_{\text{tot}}) = 23$ dB for OC reflector, and 16 dB for IRL reflector, on average.

C. Time-Frequency Lattice Response and S_{11} Responses When All SAW Tags Are Simultaneously Present in Reader Response

Simultaneous detection of all the 4 UWB SAW tags will be an important step to analyze the performance of the proposed SAW tag design and to test the orthogonality when several of them are simultaneously present and when all of them can be simultaneously detected at the same time. The simulations presented in this section will provide the proof that all the 4 interrogated SAW tags can be simultaneously detected using the time-frequency lattice approach based on our proposed tag design even when all the designed UWB SAW tags are simultaneously present in the RFID reader response.

Figs. 11–13 present the simulations for OC design and Figs. 14–16 present the simulations for the IRL design. Comparing Figs. 11 and 14, it can be seen that the IRL design shows a darker dot in the time-frequency lattice response

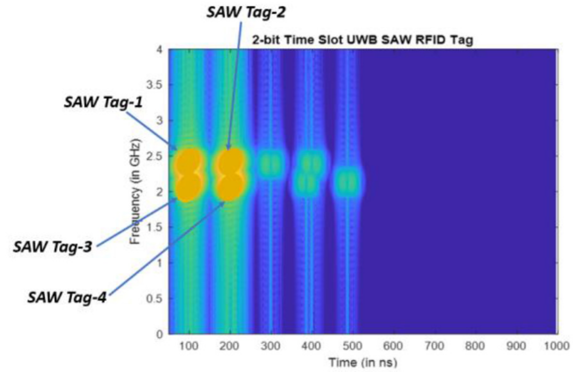

Fig. 11. Time-frequency lattice detection response when all four SAW tags are simultaneously present in the received response (OC load condition).

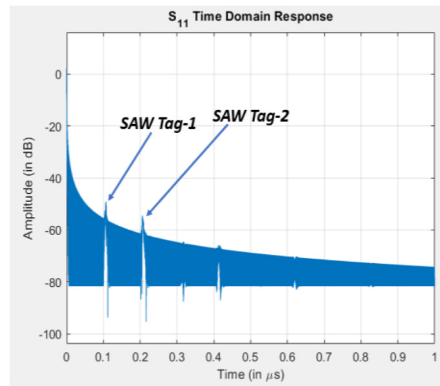

Fig. 12. S_{11} time domain response for SAW tags 1 and 2 at frequency f_1 (OC load condition).

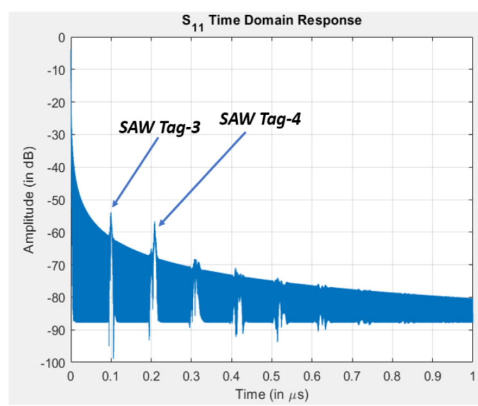

Fig. 13. S_{11} time domain response for SAW tags 3 and 4 at frequency f_2 (OC load condition).

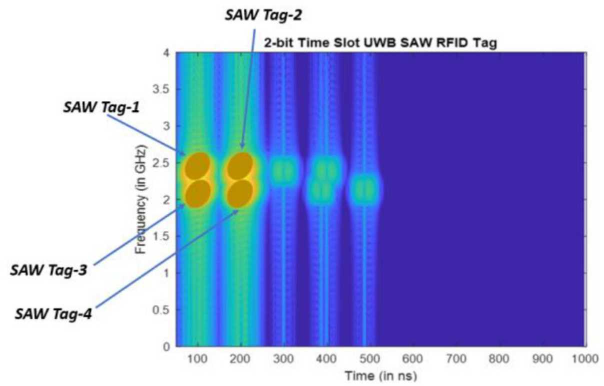

Fig. 14. Time-frequency lattice detection response when all four orthogonal SAW tags are simultaneously present in the received response (IRL load condition).

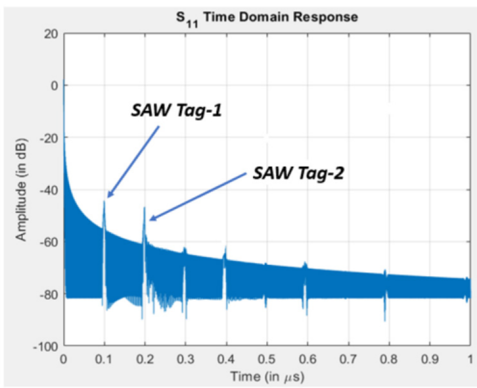

Fig. 15. S_{11} time domain response for SAW tags 1 and 2 at frequency f_1 (IRL load condition).

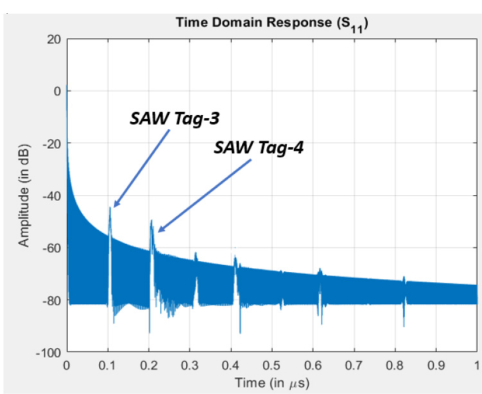

Fig. 16. S_{11} time domain response for SAW tags 3 and 4 at frequency f_2 (IRL load condition).

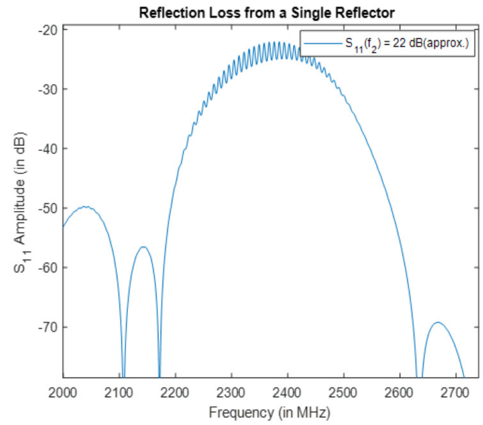

Fig. 17. Reflection loss ($S_{11}(f_2)$) for SAW tags 1 and 2 (OC load condition).

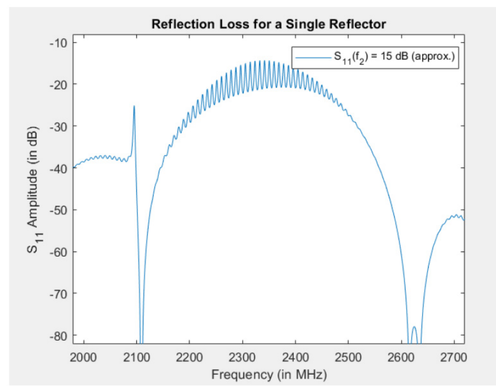

Fig. 18. Reflection loss ($S_{11}(f_2)$) for SAW tags 1 and 2 (IRL load condition).

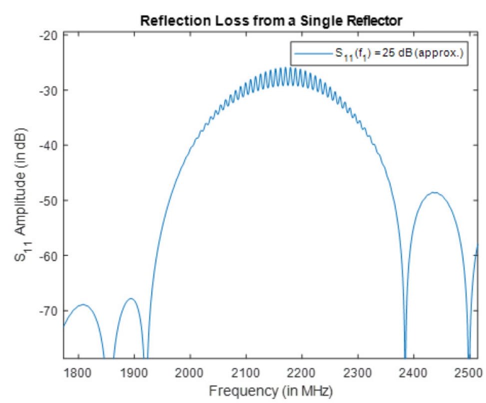

Fig. 19. Reflection loss ($S_{11}(f_1)$) for SAW tags 3 and 4 (OC load condition).

which indicates that the energy radiated from the reflecting IDT is higher than for OC reflector. The corresponding improvement can be observed in the reflection loss responses shown in Figs. 17–20 where the reflection improvement for an IRL reflector is roughly 7-dB relative to the OC reflector. The corresponding S_{11} time domain simulations for OC design are shown in Figs. 12 and 13 where the reflection amplitude is roughly -55 dB. For an IRL design, the simulation results presented in Figs. 15 and 16 show an improvement of about 7 dB indicating a -48 dB peak amplitude (roughly). The ripples around the center frequency of reflection loss is due to the triple transit effects that are present in the SAW device. However, the performance analysis and improvement in reflection loss is not affected by these effects as shown in the simulation results in Figs. 17–20. The ripples that arrive after the time-frequency signature for Figs. 11 and 14 are also due to the triple transit echoes that are inevitably present in any given SAW tag. Every yellow dot in Figs. 11 and 14 corresponds to the response from a single SAW tag. Therefore, even when all of them are simultaneously present in the response, they are not affected by these echoes since the signal strength is

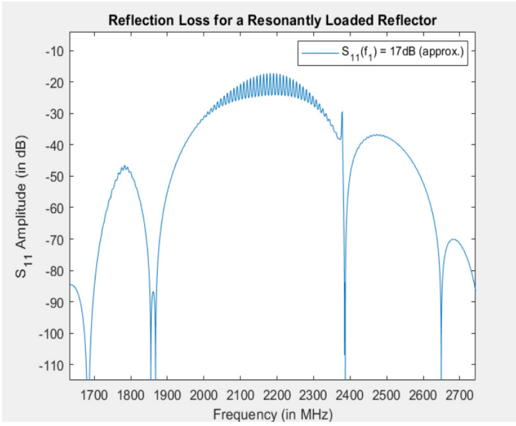

Fig. 20. Reflection loss ($S_{11}(f_1)$) for SAW tags 3 and 4 (IRL load condition).

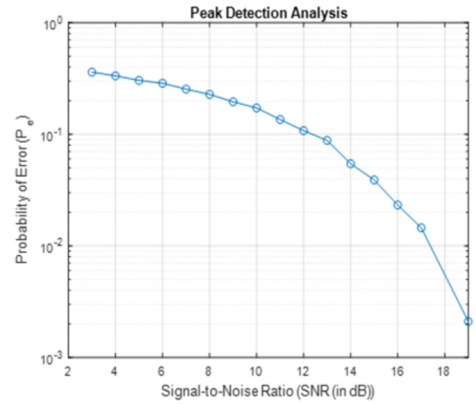

Fig. 21. Probability of error versus SNR (in dB) analysis for peak amplitude detection.

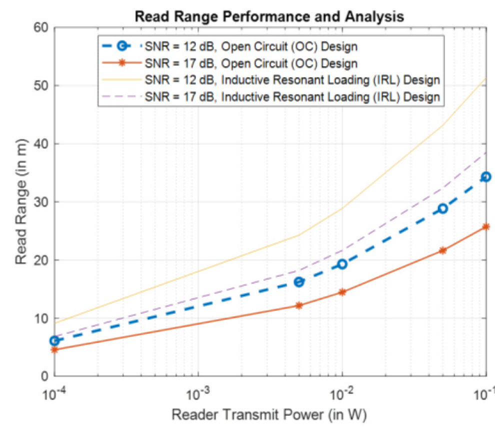

Fig. 22. Read range analysis for various reader transmit powers (in watts) for both OC and IRL load conditions.

relatively higher. When the reader receives the LFM response from the SAW tags, band-pass filtering can be used to separate it into two frequencies f_1 and f_2 to analyze them in the time-frequency lattice. To observe the S_{11} time domain responses, an inverse fast Fourier transform (IFFT) also has to be applied to the two frequency signals independently.

D. Probability of Error and Read Range analysis

A peak detection analysis is performed with respect to the time domain response of the SAW tag to analyze the detection peak performance of the tags against other spurious second-order effects and noise as shown in Fig. 21. For the case of simultaneous detection, the peaks of two SAW tags are compared against the second order effects and hence the detection threshold is set such that only the peaks that lie within ±5 dB from the strongest peaks will be considered, while the spurious reflections arising due to second-order effects and which arrive after a few microseconds will be discarded. While estimating the probability of error, every detected peak/peaks is concluded as having no error, i.e., as "count = 0" while undetected peaks are concluded as missed detection and "count = 1." After a fixed number of iterations or trials, the number of detection counts is added up and averaged over the total number of trials. The resultant fraction gives the probability of error. The dependent noise factors during the simulation include the additive white gaussian noise (AWGN) channel noise along with second-order spurious reflections that are generated within the SAW tags which are simulative of a real world cluttered environment. A threshold-based probability of detection analysis is mathematically analyzed [41].

In the light of the error probability analysis, the entire proces is repeated for varying SNR values ranging from 2 dB and up to 19 dB to represent a complete behavior. In this light, two arbitrary SNR values at error probabilities of 1 error in 10 trials and 5 errors in 1000 trials which are 12 dB and 17 dB, respectively, were taken for estimating the read range as the detectability of tags at SNR's below 12 dB was low. The read range is given by the radar [27]

$$r = \frac{\lambda}{4\pi}\sqrt[4]{\frac{P_{t,\text{reader}}.G^2_{\text{reader}}.G^2_{\text{tag}}.T_i}{L_{\text{tot}}.k.T_0.\text{SNR}}}. \tag{13}$$

From Table I, it can be shown that the read range values have been estimated for different transmit power values obeying the wireless personal area networks (WPANs) limits. The values in Table I have been plotted as shown in Fig. 22 for the corresponding SNR values 12 dB and 17 dB relating to the above mentioned error probabilities. It can be shown that many such SAW tags can be simultaneously detected from a much larger distance of up to 50 m for a reader transmit power of 100 mW. Shibata *et al.* [42], [43] achieved a read range of 6.2 m and 15 m for a reader transmit power of 20 mW. Therefore, comparing the above results with a 20 mW transmit power as in Fig. 22, we obtain a read range of approximately 34 m, which is more than double the existing read range. Therefore, we show that an IRL design acts as a better reflector in comparison to the existing designs and can guarantee a higher read range. To summarize the results, we show that it is feasible to design orthogonal SAW tags such that they can all be simultaneously detected at the same time over a wide area and with a simple reader design.

In previous results, we explained the feasibility of the time-frequency lattice-based orthogonal SAW tag design with 2 × 2 layout which results in four orthogonal SAW tags. As mentioned earlier, this is a scale-down version and that the number of orthogonal SAW tags/sensor tags can still be significantly scaled-up from 4 tags to the order of 10^6 or even billion

TABLE I
READ RANGE EVALUATION FOR BOTH THE REFLECTOR DESIGNS

Open circuit (OC) Reflector Design			Inductively Loaded Reflector (Resonant loading design)		
Input Power (in W)	Read range (in m)		Input Power (in W)	Read Range (in m)	
	SNR = 12 dB	SNR = 17 dB		SNR= 12 dB	SNR= 17 dB
100 µW	6.1	4.6	100 µW	9.1	6.8
5 mW	16.2	12.2	5 mW	24.2	18.2
10 mW	19.3	14.4	10 mW	28.9	21.7
50 mW	28.8	21.6	50 mW	43.7	32.4
100 mW	34.3	25.7	100 mW	51.3	38.5

orthogonal SAW tags with a 2×2 (2-bit) design by utilizing the cellular code-reuse approach with appropriate cluster parameter values. It is possible to use $M = 4$ cells per cluster for a 2-bit design except that there will be 1 orthogonal SAW tag and reader per cell, 4 orthogonal SAW tags per cluster, and reuse distance equal to $\sqrt{12}.R$ according to (6). By reusing this cluster with $K = 100, 1000$, and 10^6, the number of orthogonal SAW tags can be significantly scaled-up from 4 to 400, 4000, and 4 million orthogonal SAW tags. This can still be scaled-up to billions of orthogonal SAW tags. Achieving this order of magnitude was not possible with the existing SAW tag designs and the amount of increase was very limited too. Within a hexagonal cell, the maximum range with which the reader can read a SAW sensor tag is up to 38 m (approximately) at a transmit power of 100 mW for 17-dB SNR corresponding to about 5×10^{-3} error rate, and up to 51 m for 12-dB SNR corresponding to 0.1 error rate as shown in Table I. It can also be used as sensor tag if a sensing film is placed along the delay line. Intelligently reusing the same group of SAW tag ID codes at such spatially distinct hexagonal cells can help avoid the tag-to-tag interference while the reader-to-reader interference between adjacent cells can be avoided by utilizing an appropriate reader-to-reader anti-collision protocol [31]. Thus, with the combination of the proposed design approaches, it is feasible to design a wireless sensor-tag network with thousands of orthogonal SAW sensor tags and multiple readers in a cellular code-reuse infrastructure which can simultaneously sense and detect many orthogonal SAW sensor tags at a time from a long distance over a wide water body, such as ponds, lakes, rivers, or coastal areas.

VII. CONCLUSION

This article presented a feasibility study of a novel cellular code-reuse approach to deploy suitable designed orthogonal SAW sensor tags utilizing the cellular-based reader system to monitor water quality of a large water body. The SAW sensor tags being battery-free, the system has an inherent long-life advantage. The readers in the system are able to simultaneously detect numerous orthogonal SAW sensor tags at a time with the design of each reader per cell remaining simple. A generic 2×2 time-frequency lattice design and detection followed by S_{11} responses was also shown to explain that multiple orthogonal SAW tags can simultaneously be detected at a time from a longer distance by resonantly loading the IDT-based reflector. It is also worth pointing out that the advantage of cellular code-reuse approach with orthogonal SAW sensor tags can be easily extended to a WQM scenario. A reader placed in the center of a hexagon can access the ID and sensed pH variable values from multiple SAW sensor tags kept 30–50 m away at the same time using only 100 mW for less than 1 μs.

Our proposed cellular code-reuse approach for SAW tags provides two unique advantages over the traditional designs. Unlike the current anti-collision SAW tag designs where the number of orthogonal tags are few and no scalability is possible, the code-reuse approach allows the same group of SAW tag ID codes to be reused in another hexagonal cell at a predetermined distance so as to avoid tag-to-tag interference. In this way, these group of codes can be reused as many times as possible over a wide area depending on the nature of RFID application. This shows that the number of orthogonal SAW tags is scalable. Second, the scalability of orthogonal SAW tags is ensured by keeping the number of reflector time slots constant, i.e., the scalability is independent of the number of time slots the SAW tag contains. By utilizing the cellular code-reuse approach with orthogonal SAW sensor tags, we had shown that it is feasible to scale-up the number of orthogonal SAW tags and simultaneously detect all of them at a time from a distance and over a wide area. The cellular code-reuse approach is practically feasible and does not necessarily require an experimental validation as the concept is inspired from frequency reuse which is universally applied in today's mobile communication networks.

VIII. FUTURE WORK

The proposed cellular code-reuse approach for SAW sensor tags is the first and unique technique to significantly maximize the number of orthogonal codes in them. Unlike existing work, this approach allows us to scale-up the number of orthogonal SAW sensor tags to any figure of interest, to even more than million or billion codes when required. Besides that, certain limitations and issues deserve additional attention, which can be addressed as part of the future work in SAW RFID tags.

1) The number of time slots in SAW tags cannot be indefinitely increased due to two losses namely the: a) SAW propagation loss and b) diffraction loss, which results in the bending of SAW waves around the edges of the reflecting IDT. SAW propagation loss is a function of distance and is an inevitable consequence resulting due to increasing the number of reflector time slots. But it can be resolved by further improving the reflectivity of SAW tag reflectors. Diffraction loss can be mitigated by appropriately designing the reflecting IDT such that the wavelength of SAW wave is sufficiently smaller than the acoustic aperture.
2) This work uses a bidirectional IDT which radiates SAW wave equally in both directions resulting a total of −6-dB loss. However, this can be resolved by utilizing a unidirectional IDT which radiates the SAW wave in only one direction thereby contributing to only a total

of −3-dB loss. This will accordingly reduce the reflection loss and further extends the read range compared to a bidirectional reflecting IDT.

3) This work also utilized a resonant loading based on inductor that can maximize the read range relative to an OC reflecting IDT. However, loading the inductor across the reflecting IDT requires an additional work during the fabrication process which also increases the overall cost per SAW tag. But this additional increase in cost can be reduced or even further through the use of silicon-based multilayer substrates or polyvinylidene fluoride (PVDF) [44], [45] in conjunction with an appropriate choice of fabrication technique. Thus, the components, such as the antenna and the inductor for resonant loading can be built and integrated with reflecting IDTs on the same low-cost substrate which reduces the cost per SAW tag and as a bulk.

References

[1] C. G. Panayiotou, D. Fatta, and M. P. Michaelides, "Environmental monitoring using wireless sensor networks," Dept. Elect. Eng., Univ. Cyprus, Nicosia, Cyprus, Tech. Rep., 2005. [Online]. Available: http://www.eng.ucy.ac.cy/christos/Papers/PFM_WMCCS.pdf

[2] K. S. Adu-Manu, C. Tapparello, W. Heinzelman, F. A. Katsriku, and J.-D. Abdulai, "Water quality monitoring using wireless sensor networks: Current trends and future research directions," *ACM Trans. Sensor Netw.*, vol. 13, no. 1, p. 4, Jan. 2017.

[3] D. Chapman, *Water Quality Assessments: A Guide to the Use of Biota, Sediments and Water in Environmental Monitoring*, 2nd ed. Cambridge, U.K.: Cambridge Univ. Press, 1996.

[4] D. Estrin, A. Sayeed, and M. Srivastava, "Wireless sensor networks," in *Proc. 8th ACM Int. Conf. Mobile Comput. Netw. (MobiCom)*, vol. 255. Atlanta, GA, USA, 2002, pp. 1–32. [Online]. Available: https://disalw3.epfl.ch/teaching/swarm_intelligence/ay_2006-07/exercises/SI_06-07_labhwk09_tutorial.pdf

[5] J. Cotruvo. *Hardness in Drinking-Water: Background Document for Development of WHO Guidelines for Drinking-Water Quality*. Nov. 12, 2016. [Online]. Available: http://www.who.int/water_ sanitation_health/dwq/chemicals/hardness.pdf

[6] USGS. (2015). *The World's Water*. Nov. 12, 2016. [Online]. Available: http://water.usgs.gov/edu/earth wherewater.html

[7] R. Yue and T. Ying, "A water quality monitoring system based on wireless sensor network and solar power supply," in *Proc. IEEE Int. Conf. Cyber Technol. Autom. Control Intell. Syst. (CYBER)*, Los Alamitos, CA, USA, 2011, pp. 126–129.

[8] Y. Derbew and M. Libsie, "A wireless sensor network framework for large-scale industrial water pollution monitoring," in *Proc. IST-Africa Conf.*, Los Alamitos, CA, USA, 2014, pp. 1–8.

[9] K. Farrell-Poe. (2005). *Water Quality and Monitoring*. [Online]. Available: https://cals.arizona.edu/watershedsteward/resources/docs/guide/(10)Water%20Quality.pdf

[10] P. Jiang, H. Xia, Z. He, and Z. Wang, "Design of a water environment monitoring system based on wireless sensor networks," *Sensors*, vol. 9, no. 8, pp. 6411–6434, 2009.

[11] D. N. Myers, "Why monitor water quality?," Environment, U.S. Geol. Survey, Reston, VA, USA, Dec. 24, 2020. https://water.usgs.gov/owq/WhyMonitorWaterQuality.pdf

[12] C. Herrojo *et al.*, "Time-domain-signature chipless RFID tags: Near-field chipless-RFID systems with high data capacity," *IEEE Microw. Mag.*, vol. 20, no. 12, pp. 87–101, Dec. 2019.

[13] D. Enguang, "State-of-the-art instruments based upon SAW wireless tags, SAW match filters, and SAW resonators," in *Proc. IEEE Ultrason. Symp. Int. Symp.*, vol. 1. Tahoe, NV, USA, 1999, pp. 425–428.

[14] V. Plessky, T. Ostertag, V. Kalinin, and B. Lyulin, "SAW-tag system with an increased reading range," in *Proc. IEEE Int. Ultrason. Symp.*, San Diego, CA, USA, 2010, pp. 531–534.

[15] R. Shi *et al.*, "SAW tags with enhanced penetration depth for buried assets identification," *IEEE Trans. Ind. Electron.*, early access, Aug. 25, 2020, doi: 10.1109/TIE.2020.3018056.

[16] W. Liu, J. Xing, and L. Xie, "Matrix method for multiple wireless orthogonal frequency-coded SAW sensor tags identification," *IEEE Sensors J.*, vol. 16, no. 10, pp. 3834–3847, May 2016.

[17] N. Saldanha and D. C. Malocha, "Pseudo-orthogonal frequency coded wireless SAW RFID temperature sensor tags," *IEEE Trans. Ultrason., Ferroelectr., Freq. Control*, vol. 59, no. 8, pp. 1750–1758, Aug. 2012.

[18] T. Han, W. Wang, H. Wu, and Y. Shui, "Reflection and scattering characteristics of reflectors in SAW tags," *IEEE Trans. Ultrason., Ferroelectr., Freq. Control*, vol. 55, no. 6, pp. 1387–1390, Jun. 2008.

[19] N. A. Cloete, R. Malekian, and L. Nair, "Design of smart sensors for real-time water quality monitoring," *IEEE Access*, vol. 4, pp. 3975–3990, 2016.

[20] L. Kuang, P. Shi, C. Hua, B. Chen, and H. Zhu, "An enhanced extreme learning machine for dissolved oxygen prediction in wireless sensor networks," *IEEE Access*, vol. 8, pp. 198730–198739, 2020.

[21] T. P. Lambrou, C. C. Anastasiou, C. G. Panayiotou, and M. M. Polycarpou, "A low-cost sensor network for real-time monitoring and contamination detection in drinking water distribution systems," *IEEE Sensors J.*, vol. 14, no. 8, pp. 2765–2772, Aug. 2014.

[22] C. Hartmann, P. Hartmann, P. Brown, J. Bellamy, L. Claiborne, and W. Bonner, "Anti-collision methods for global SAW RFID tag systems," in *Proc. IEEE Ultrason. Symp.*, vol. 2. Montreal, QC, Canada, 2004, pp. 805–808.

[23] M. Brandl, S. Schuster, S. Scheiblhofer, and A. Stelzer, "Anti-collision technique of SAW ID tags at unknown temperature using integer programming," in *Proc. IEEE Int. Ultrason. Symp.*, Rome, Italy, 2009, pp. 698–701.

[24] M. Brandl, S. Schuster, S. Scheiblhofer, and A. Stelzer, "A new anti-collision method for SAW tags using linear block codes," in *Proc. IEEE Int. Freq. Control Symp.*, Honolulu, HI, USA, 2008, pp. 284–289.

[25] Y.-Y. Zhong, Z.-J. Chen, X. Wang, C. Han, and J. Fu, "Anti-collision SAW tags based on CIDT," in *Proc. Symp. Piezoelect. Acoustic Waves Device Appl. (SPAWDA)*, Jinan, China, 2015, pp. 137–142.

[26] A. V. Sorokin and D. A. Shepeta, "Time-frequency approach to anti-collision signal processing for RFID SAW tags," in *Proc. Wave Electron. Appl. Inf. Telecommun. Syst. (WECONF)*, St. Petersburg, Russia, 2019, pp. 1–4.

[27] K. Suresh, V. Jeoti, and M. Drieberg, "A read range maximization approach for UWB surface acoustic wave (SAW) RFID tags based on interdigital transducer (IDT) as a reflector," in *Proc. IEEE 6th World Forum Internet Things (WF-IoT)*, New Orleans, LA, USA, 2020, pp. 1–6.

[28] W. Liu, B. Tan, and Y. Gong, "SAW temperature sensors system for smart electric grid," in *Proc. IEEE Int. Ultrason. Symp.*, San Diego, CA, USA, Oct. 2010, pp. 756–759.

[29] R. Tang *et al.*, "PH measurements with ZvO based surface acoustic wave resonator," in *Proc. 16th Int. Solid-State Sensors Actuators Microsyst. Conf.*, Beijing, China, 2011, pp. 1132–1135.

[30] T. S. Rappaport, *Wireless Communications: Principles and Practice, Prentice Hall Communications Engineering and Emerging Technologies Series*. London, U.K.: Dorling Kindersley, 2009.

[31] Z. Li, G. He, and S. Wang, "NFRA-AIC: A RFID reader anti-collision protocol with adaptive interrogation capacity," *IEEE Access*, vol. 7, pp. 86493–86509, 2019.

[32] Y. Wang, D. Chen, W. Liu, X. Chen, X. Liu, and J. Xie, "An AlN based SAW device for detection of impurities in water based on measuring the signal-to-noise ratio," in *Proc. IEEE 13th Annu. Int. Conf. Nano/Micro Eng. Molecular Syst. (NEMS)*, Singapore, 2018, pp. 90–93.

[33] Safaa M. Al-Hilli, M. Willander, A. ʿOst, and P. Strâlfors "ZnO nanorods as an intracellular sensor for pH measurements," *J. Appl. Phys.*, vol. 102, Oct. 2007, Art. no. 084304.

[34] F. Adamo, F. Attivissimo, C. G. C. Carducci, and A. M. L. Lanzolla, "A smart sensor network for sea water quality monitoring," *IEEE Sensors J.*, vol. 15, no. 5, pp. 2514–2522, May 2015.

[35] A. C. D. S. Júnior, R. Munoz, M. D. L. Á. Quezada, A. V. L. Neto, M. M. Hassan, and V. H. C. D. Albuquerque, "Internet of Water Things: A remote raw water monitoring and control system," *IEEE Access*, vol. 9, pp. 35790–35800, 2021.

[36] S. O. Olatinwo and T. H. Joubert, "Enabling communication networks for water quality monitoring applications: A survey," *IEEE Access*, vol. 7, pp. 100332–100362, 2019.

[37] S. O. Olatinwo and T. Joubert, "Energy efficient solutions in wireless sensor systems for water quality monitoring: A review," *IEEE Sensors J.*, vol. 19, no. 5, pp. 1596–1625, Mar. 2019.

[38] Dr. A. Wilzeck, Dr. M. D. Perez Guirao, and Dr. E. Dimitrov, "UWB Technology and Regulation," wiseSense GmbH, Hanover, Germany, White Paper. [Online]. Available: https://ecfsapi.fcc.gov/file/60001090750.pdf
[39] D. P. Morgan, *Surface Acoustic Wave Filters: With Applications to Electronic Communications and Signal Processing*, 2nd ed. Amsterdam, The Netherlands: Elsevier, 2007.
[40] S. Harma, V. P. Plessky, X. Li, and P. Hartogh, "Feasibility of ultra-wideband SAW RFID tags meeting FCC rules," *IEEE Trans. Ultrason., Ferroelectr., Freq. Control*, vol. 56, no. 4, pp. 812–820, Apr. 2009.
[41] G. Cerda-Villafana and Y. S. Shmaliy, "Thresholds for the identification of commercial wireless SAW ID-tags," in *Proc. 1st Int. Conf. Sensor Device Technol. Appl.*, Venice, Italy, 2010, pp. 226–231.
[42] K. Shibata *et al.*, "Long range wireless SAW passive tag system using patch antenna for vibration monitoring," in *Proc. Asia-Pac. Microw. Conf. (APMC)*, Kyoto, Japan, 2018, pp. 1417–1419.
[43] K. Shibata *et al.*, "Long range wireless SAW passive tag system for vibration monitoring," in *Proc. IEEE Int. Ultrason. Symp. (IUS)*, Washington, DC, USA, 2017, pp. 1–4.
[44] K. Suresh, V. Jeoti, S. Soeung, M. Drieberg, M. Goh, and M. Z. Aslam, "A comparative survey on silicon based and surface acoustic wave (SAW)-based RFID tags: Potentials, challenges, and future directions," *IEEE Access*, vol. 8, pp. 91624–91647, 2020.
[45] J. Chen, J. Zhao, L. Lin, and X. Sun, "Truncated conical PVDF film transducer for air ultrasound," *IEEE Sensors J.*, vol. 19, no. 19, pp. 8618–8625, Oct. 2019.

Kasyap Suresh received the B.Eng. degree in electronics and communication engineering from Anna University, Chennai, India, in 2017. He is currently pursuing the M.S. degree in electrical and electronics engineering with Universiti Teknologi PETRONAS (UTP), Seri Iskandar, Malaysia, where he conducts research in the Communications Lab.

He is affiliated with the Communications Cluster Group, UTP. His research interests include battery-free sensing and tags, interference-free networks, location-based services, and various applications of signal processing and communications.

Varun Jeoti (Senior Member, IEEE) received the Ph.D. degree from the Indian Institute of Technology (IIT) Delhi, New Delhi, India, in 1992.

He worked on several sponsored R&D projects with IIT-Delhi and IIT-Madras, Chennai, India, from 1980 to 1989. He used to be a Visiting Faculty with the Electronics Department, Madras Institute of Technology, Anna University, Chennai, from 1989 to 1990. In 1995, he joined the Delhi Institute of Technology, New Delhi, for the 5 years. He moved to School of Electrical and Electronics Engineering, Universiti Sains Malaysia, George Town, Malaysia, in 1995. In 2001, he joined the Department of Electrical and Electronics Engineering, Universiti Teknologi PETRONAS, Seri Iskandar, Malaysia. He is currently the ERA Chair with the University of Novi Sad, Novi Sad, Serbia, to lead the research efforts in the field of Stretchable and Textile Electronics. His research interests include, among others include signal processing, surface acoustic wave (SAW) devices, wearable sensors, sensor tags, SAW sensors/microfluidics, and wireless communications for various applications.

Micheal Drieberg (Member, IEEE) received the B.Eng. degree in electrical and electronics engineering from Universiti Sains Malaysia, George Town, Malaysia, in 2001, the M.Sc. degree in electrical and electronics engineering from Universiti Teknologi PETRONAS (UTP), Seri Iskandar, Malaysia, in 2005, and the Ph.D. degree in electrical and electronics engineering from Victoria University, Melbourne, VIC, Australia, in 2011.

He is currently a Senior Lecturer with the Department of Electrical and Electronics Engineering, UTP. He has authored and co-authored several IEEE journals and conferences. His research interests include radio resource management, medium access control protocols, energy harvesting communications, and performance analysis for wireless sensor networks.

Dr. Drieberg served as a reviewer for IEEE journals and conferences. He has also made several contributions to the IEEE 802.16d Task Group.

Socheatra Soeung (Member, IEEE) was born in Phnom Penh, Cambodia, in 1986. He received the B.Eng. degree (Hons.) in electrical and electronic, major in computer system architecture from Universiti Teknologi PETRONAS (UTP), Seri Iskandar, Malaysia, in 2010, and the M.Sc. and Ph.D. degrees in PCB testing based on Eddy current from UTP in 2013 and 2018, respectively.

He is currently holding the lecturer position with UTP, where he currently holds faculty position with the Department of Electrical and Electronics Engineering. His research interests include lossy filter design, passive microwave filter design, and multiband filter design.

Dr. Soeung is an MTT member and a committee member of the IEEE ED/MTT/SSC Penang Chapter, Malaysia.

Asif Iqbal received the B.E. degree in telecommunication engineering from Allama Iqbal Open University, Islamabad, Pakistan, in 2006, and the M.Sc. degree in electrical and electronic engineering from the Universiti Teknologi PETRONAS, Seri Iskandar, Malaysia, in 2012, where he is currently pursuing the Ph.D. degree.

His main research interests include channel sounding techniques, wireless system design, Internet of Things, and the channel modeling using numerical methods of wireless systems. He has done a number of experiments and projects by measuring the wireless signals for maritime wireless communications.

Goran M. Stojanović (Member, IEEE) received the B.Sc., M.Sc., and Ph.D. degrees in electrical engineering from the Faculty of Technical Sciences (FTS), University of Novi Sad (UNS), Novi Sad, Serbia, in 1996, 2003, and 2005, respectively.

He is a Full Professor with FTS, UNS. He has authored 260 articles, including 98 in leading peer-reviewed journals with impact factors, five books, three patents, and one chapter in monograph. He is a keynote speaker for 12 international conferences and has over 13 years' experience in coordination of EU funded projects (H2020, FP7, EUREKA, ERASMUS, and CEI), with total budget exceeding 14.86 MEUR. His research interests include sensors, microfluidics, and flexible electronics.

Sohail Sarang (Student Member, IEEE) received the bachelor's degree in telecommunication engineering from Hamdard University, Karachi, Pakistan, in 2014, and the master's degree in electrical and electronics engineering by research from Universiti Teknologi PETRONAS, Seri Iskandar, Malaysia, in 2018. He is currently pursuing the Ph.D. degree with the Faculty of Technical Sciences, University of Novi Sad, Novi Sad, Serbia.

He is currently working as a Marie Curie Early-Stage Researcher in H2020 AQUASENSE ITN project. His research interests include wireless sensor networks, including medium access control protocols, energy harvesting communications, and quality of service in sensor networks.